euspen's 22nd International Conference & Exhibition, Geneva, CH, May/June 2022
www.euspen.eu

Simulation and accuracy evaluation of a new 3D photogrammetric position measurement system

Uwe Bielke[1,2], Luis Garcia[3], David K. Harrison[1], Theo Hageney[2], Klaus Banzhaf[2], Ernst Wiedenmann[4], Rainer Börret[3]

[1]*Glasgow Caledonian University, Glasgow, United Kingdom*
[2]*eμmetron GmbH, Aalen, Germany*
[3]*University of Aalen, Aalen, Germany*
[4]*Serious Enterprises GmbH, Aalen, Germany*

Ubielk200@caledonian.ac.uk

Abstract

Automated handling systems are well integrated into today's production processes. However, production processes like 3D printing, monitoring moving objects, gluing, or welding require handling systems with high precision and repeatability. Thus, a calibration of the handling system is necessary to achieve the needed accuracies. Furthermore, to maintain the flexibility of the handling systems, such as industrial robots, the correction process needs to be done online. This leads to the demand for measurement systems with the ability to measure at a high sample rate, high accuracy and high repeatability at the same time.

This article discusses a new photogrammetric approach using an aperture array and a single camera, which can provide online 3D data of a machine under test. Previous photogrammetric methods needed a multi-camera solution to achieve an online TCP measurement with an accuracy below 10 µm. However, these systems had high spatial demand and a high need to synchronise and calibrate the used camera systems. Thus, the new Multi-Aperture-Positioning-System (MAPS) offers the advantages of a single camera system and the features and precision of a multi-camera system with the benefit of being cheap, modular and scalable.

The MAPS measurement system is based on a single camera and a light-emitting target. The setup includes an LED target, the aperture mask and the camera sensor. The light emitted by the LED target travels through the holes in the aperture mask and creates light spots in the image plane. The light source coordinates can then be determined by calculating the intersection point of the lines defined by the holes in the aperture mask and the corresponding light spot positions on the sensor.

In the following paper, the accuracy of the MAPS measurement system is discussed. Therefore, the occurring errors of the measurement system are measured by using a highly accurate positioning system. These errors are described and identified using a simulation of the measurement system.

Photogrammetry, 3DoF measurement, online measurement, TCP, accuracy, robotics, online calibration

1. Introduction

Driven by economic interests, the modern consumer markets demands for individualised products is changing the production processes, from mass production to small batch sizes of highly individualised products. Shorter product life cycles, requiring short-production ramp-up times, result from that development. Therefore, product quality can no longer be evaluated over time. For this reason, the absolute accuracy of machine tools is of increasing importance [*1*]. Processes adapted to this demand require machines with high repeatability. To achieve the needed geometric accuracy, it is possible to correct them in a feedback loop [*2*] or by accurately calibrating the machine tool using a correction matrix [*3*]. The coordination of different machines is another need these new production processes have. Therefore, all devices used in these processes need to work within the same coordinate system, and their position needs to be known precisely within this coordinate system. For example, in assembling processes, the parts that need to be joined are mounted by different handling systems. If these systems are not perfectly aligned, the product can be damaged during the assembly. To avoid this, all machines and workpieces in the process need to be measured precisely in the same coordinate system.

Measurement systems available today, such as Laser Tracker or photogrammetric methods, cannot achieve online measurement, high accuracy, and the possibility to measure multiple systems simultaneously at the same time. For example, Laser Trackers offer very high precision and high measurement frequencies compared to photogrammetric methods. But due to the need for a particular target that reflects the laser light emitted by the Laser Tracker, these systems cannot measure multiple targets simultaneously [*4–10*]. Compared to that, measurement systems based on photogrammetry, such as described in [*8*, *9*, *11–15*], excel at measuring numerous targets simultaneously. But due to limitations with camera systems, such as a limited viewing angle, a limited sensor resolution combined with aberrations caused by the used optics, photogrammetric systems lack accuracy compared to a Laser Tracker. Another limitation caused by the used camera systems is the trade-off between high framerate and high-resolution

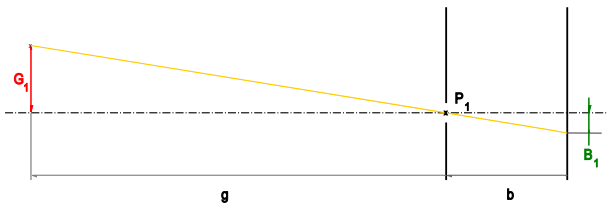

Figure 1: Sketch of a Pinhole Camera. P1 represents the pinhole. G1 is the object height; B1 is the height of the image; g is the distance from the object to the pinhole; b is the distance from the pinhole to the display.

images. Therefore, these systems are slower than a Laser Tracker.

This article will introduce a new photogrammetric measurement method, the Multi-Aperture-Positioning-System, capable of online measuring different machines under test while delivering high accuracy measurements. The setup for MAPS consists of a LED target, an aperture mask and a single camera sensor.

2. The Multi-Aperture-Positioning System

The Multi-Aperture-Positioning-System (MAPS) is based upon the principle of a pinhole camera. Despite the straightforward structure, the pinhole camera has some advantages in optical imaging. According to [*16*, *17*], the pinhole camera has no distortion, an extreme wide angular field and a wide depth of focus. Therefore, a straight line can be drawn between the light source/ object, the pinhole and the corresponding image.

The height of the image of the object on the image plane can be calculated using the intercept theorem. Figure 1 shows a sketch where the intercept theorem for the pinhole camera is displayed. The following Equation (2) for the magnification factor β can be established based on this theorem.

$$\beta = \frac{|B_1|}{|G_1|} = \frac{|b|}{|g|} \tag{1}$$

Where B_1 stands for the object's size, G_1 for the size of the image, b represents the distance from the pinhole to the image plane and g gives the distance from the object to the pinhole. Equation (1) shows that the magnification factor β, which depends on the lengths b and g and not on the pinhole size. Since equation (2) has two unknown variables, this Equation cannot be solved for G_1 or g independently. A second hole gives a second equation solving this problem, and G1 and g can be calculated. This technique is described in the following chapter.

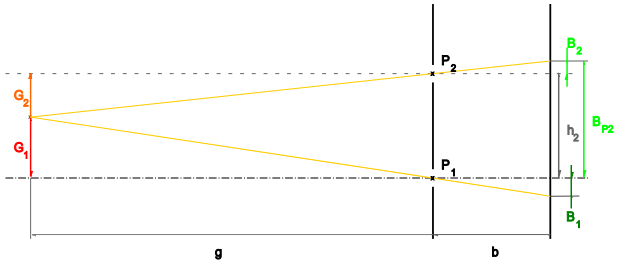

Figure 2: Sketch of the Multi-Aperture Technique. A second pinhole is added in comparison to Figure 1. The second pinhole P_2 has the distance h_2 from the pinhole P_1. Resulting from this a second straight line can be evaluated with a new object height G_2 and a new image height B_2. B_{P2} is the image height relative to the first pinhole P_1.

2.1. Multi-Aperture Technique

Following Equation (1), one can recognise that for a fixed distance *b* from the pinhole to the imaging plane, the size of image *B* is only dependant on the object-related parameters *g* and G_1. By adding a second hole into the aperture mask, observing the same light source, a second straight line can be calculated intersecting the first straight line in the position of the light source. In Figure 2, a second pinhole is added to the sketch displayed in Figure 1 with a distance of h_2 in respect to the already existing one. This results in a second formula given by equation (2).

$$\beta = \frac{|B_2|}{|G_2|} = \frac{|b|}{|g|} \tag{2}$$

Since the variables related to the z-axis, b and g, are the same as in Equation (1), only the variables connected to the x- or y-axis differ. B_{P2} gives the height of the second light spot relative to the optical axis, which is perpendicular to the aperture mask and passes right through hole P_1. Thus, the image height B_2 can be expressed as follows,

$$B_2 = B_{P2} - h_2 \tag{3}$$

where B_{P2} is the image height relative to the optical axis, the image height relative to a straight line perpendicular to the aperture mask G_2 can be calculated as shown in Equation (4).

$$G_2 = h_2 - G_1 \tag{4}$$

Using Equation (3) and Equation (4) to replace B_2 and G_2 in Equation (2), it becomes

$$\frac{|B_{P2}| - h_2}{h_2 - |G_1|} = \frac{|b|}{|g|} \tag{5}$$

where G_1 and g are the unknown variables expressed by the results of a second pinhole. B_{P2} can be evaluated by finding the peak of a light spot and its coordinates in the image plane. Substitution of $\frac{|b|}{|g|}$ with Equation (1) results in the following expression

$$\frac{|B_1|}{|G_1|} = \frac{|B_{P2}| - h_2}{h_2 - |G_1|} \tag{6}$$

solving for G_1 results in Equation (7).

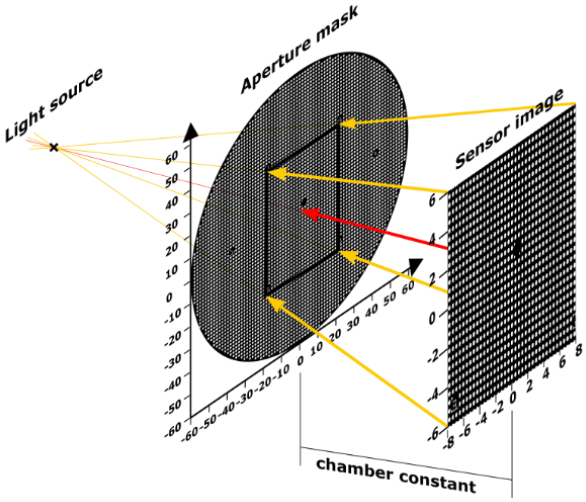

Figure 3: Sketch of the measurement principle of MAPS using vector analysis. The light emitted by the LED target passes the aperture mask, containing holes arranged on a grid and is measured by a camera sensor behind the aperture mask.

$$G_1 = \frac{h_2 \cdot |B_1|}{|B_1| + |B_{P2}| - h_2} \tag{7}$$

Thus, G_1 depends only on the offset of the second pinhole h_2 and the relative image height B_1 depending on the first pinhole and the relative image height B_{P2}. Using Equation (7) to calculate G_1 and solving Equation (1) for $|g|$, the object distance $|g|$ can be calculated. Thus, using two Pinholes, the object-related parameters for the height $|G|$ and the distance to the pinhole $|g|$ can be calculated when the image related parameters (B_1, B_2, h_1, h_2 and b) are known. Based on this principle, the MAPS system can calculate the position of a light source in space.

Another view on the multi-aperture technique is represented by vector analysis instead of the intercept theorem. Therefore, the location vector $\overrightarrow{OP_{\mathrm{spot,n}}}$ is calculated by using the spot centre coordinates P_{spot}. Since every spot measured with the sensor can be correlated to one specific hole in the aperture mask, a direction vector $\overrightarrow{P_{spot,n}P_{hole,n}}$ from the spot, the centre coordinates $P_{spot,n}$ to the hole centre coordinates $P_{hole,n}$ can be calculated. Therefore, the line $\overrightarrow{g_n}$ can be written as follows

$$\begin{aligned}\vec{g}_n &= \overrightarrow{OP_{\mathrm{spot,n}}} + r \cdot \overrightarrow{P_{spot,n}P_{hole,n}} \\ &= P_{spot,n} + r \cdot (P_{spot,n} - P_{hole,n})\end{aligned} \tag{8}$$

where r can be any real number. A typical sensor image contains between 700 and 1000 spots (N_{spots}) and therefore, the same amount of line equations can be formulated. The number of light spots visible on the sensor depends on the distance of the light source from the aperture mask, the chosen chamber constant, and the size of the sensor. To display the behaviour of the calculated lines, Figure 3 shows a sketch of the measurement principle using vector analysis. Therefore, on the left side, the point light source is represented by a cross. In the centre part of the sketch, the aperture mask is shown, and on the right side, the image is plotted at the sensor position. Five of those lines related to the corners and the centre of the sensor image are shown in Figure 3. It is also shown that all of those straight lines intersect in the position of the light source. This behaviour can be exploited by calculating the intersection point of all lines. As it can be seen in Figure 3, all vectors $\vec{g}_n$ point towards the light source position. This relation can be used to evaluate the light source coordinates by calculating the intersection point of the vectors.

Since only two vectors are needed to calculate an intersection point, it is possible to calculate multiple intersection points using multiple vector pairs. Therefore, the number of possible calculations for the coordinates of the LED target can be calculated, as shown in Equation (1).

$$C_k(N_{spots}) = \binom{N_{spots}}{k} = \frac{N_{spots}!}{k!\,(N_{spots} - k)!} \tag{9}$$

Where $C_k(n)$ is the number of combinations without repetition, k is the number of elements to combine. This results in a total number of ~240 000 to 500 000 positions that can be calculated from a single measurement. The gain of accuracy in comparison to a single pair of lines can be calculated by $\sqrt{N_{spots} - 1}$ and therefore, the accuracy gain can be estimated by a factor between 26 and 32.

The downside of this technique is the increase in computation time. To calculate the LED position, it is necessary to determine the centre of the light spots in the image. After that, the corresponding hole in the aperture mask has to be found. These calculation steps increase linearly with an increasing number of spots N_{spots} in the image. Finally, the intersections between the evaluated straight lines have to be calculated. Since there are $C_k(n)$ possible intersections, the computation time of this step increases linearly to $C_k(n)$.

3. Proof of concept

3.1. Setup

For proof of concept, a prototype setup was realised using an Allied Vision Prosillica GT-3300 with a framerate of around four frames per second. The resolution of this sensor is 3296 x 2472 pixels with square pixels with a pixel pitch of 5.5 µm, resulting in a sensor area of roughly 18.13 mm times 13.6 mm. As an aperture mask, a 1 mm thick glass plate with a diameter of 150mm is used. To create a mask with multiple apertures, the glass plate is coated with chromium layer containing holes placed in a grid with a hole distance of nominal 0.4785 mm and a hole diameter of nominal 0.1595 mm. The area, including the apertures, measures 120 mm in diameter and contains approximately 42 000 holes. As a light source, a Cree LED Xlamp XQ-E Royal Blue was used with a wavelength of 450nm. This light source is mounted to a Zeiss PRISMO Access with a Zeiss Vast XT measurement head. This coordinate measurement system has a specification for length measurement error $E_{0,\mathrm{MPE}}$ of 1.2 µm + L / 500 and a useable measurement area of 0,9 m x 1,2 m x 0,7 m.

As displayed in Figure 4 a), the MAPS setup is placed on a 50 mm thick aluminium plate and mounted on the granite plate of the CMM, therefore, extending the working area of the CMM in a way that the functional area of the CMM stays the same. The black box mounted on the aluminium plate contains the MAPS prototype setup, including the aperture mask and the camera sensor. This box is needed to protect the system from stray light and dust particles.

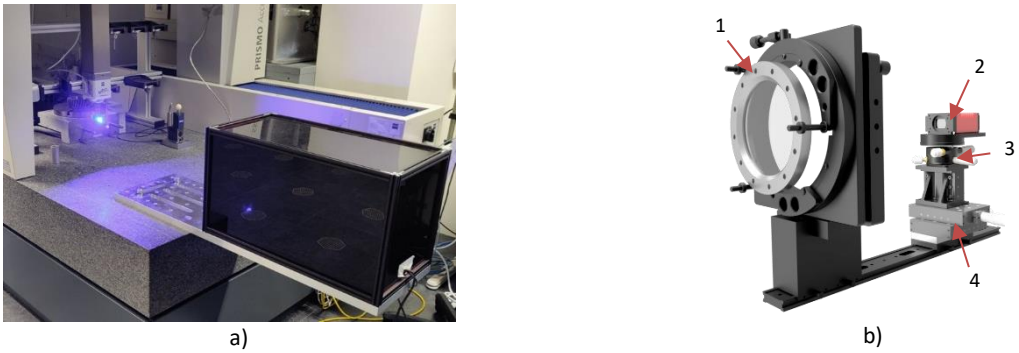

a) b)

Figure 4: Experimental setup for MAPS. a) Image of the experimental setup. The LED Target is mounted on a Zeiss PRISMO Access equipped with a Zeiss VAST XT measurement head. The black box contains the MAPS setup and protects it from stray light and dust. It is also visible that the MAPS is positioned on an aluminium plate that extends the working area of the CMM to keep the measurement area. b) Sketch of the MAPS setup build inside the black box in Figure 4 a). 1) is the aperture mask. 2) the used Allied Vision Prosillica GT-3300. 3) is a tip- tilt stage to align the sensor against the aperture mask. 4) is a x- y- and z- stage to position the camera sensor in front of the aperture mask.

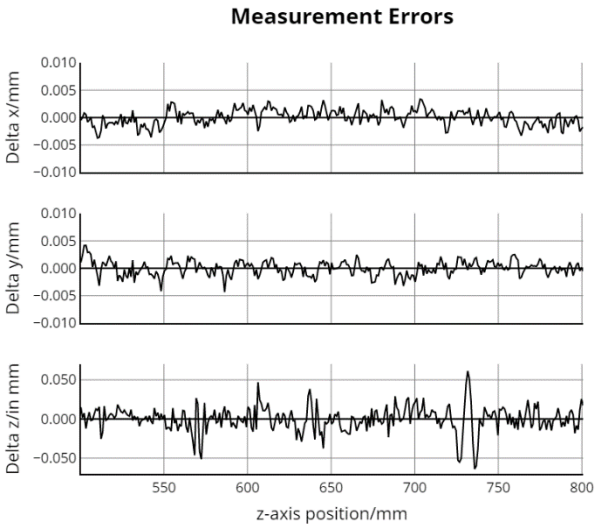

Figure 5: Experimental results of a line measurement conducted using a ZEISS PRISMO Access CMM as a positioning system. The measured line is placed in such a way, that the line equals the optical axis of MAPS. Displayed are the deviations between the measured position and the position given by the CMM. Each position is measured 20 times and the RMS coordinates are calculated. The plot for Delta z shows multiple spikes.

To verify the accuracy of MAPS at different distances, a line measurement was carried out, where the line was placed on the optical axis of MAPS. The distance of the LED was chosen from 400 mm to 800 mm with a step width of 1 mm. At every step, 20 different measurements were performed.

3.2. Results

Figure 5 displays the experimental results. Three different graphs are shown for the difference between the x-, y- and z-coordinates of the measured MAPS values and the corresponding actual positions given by the CMM. The RMS values for these line plots are 1.4 µm for the x-coordinate, 1.4 µm for the y-coordinate and 25 µm for the z-coordinate. In these RMS values, the accuracy of the CMM is included, which is in a similar scale.

The line plot for the z-error thereby shows spikes not visible for the x- and y- error plots. Two spikes can be found at a z-axis position of ~570 mm and ~730 mm. These spikes range over approximately 20 mm and have a peak to valley distance of up to 130 µm.

4. Simulation

In the full paper, the previously described spikes are analysed using a MAPS simulation. Therefore, single spots are simulated, and the algorithms' resulting error is discussed. In addition to that, the MAPS measurements are simulated fully and lead to a better understanding of the new measurement technique.

5. Conclusion

A newly developed optical measurement device measuring the coordinates of a light source has been described. This measurement system aims to measure the machine errors of a handling system, for example, a machine tool, a coordinate measurement machine or a robot. Three-dimensional data can be obtained using a single light source. Since the Multi-Aperture-Positioning System can measure the position of any light source, which fulfils the necessary brightness requirements, a target can be created that allows for measuring all six degrees of freedom. Therefore at least three LEDs are required. Another advantage of the independence of the used light source is that the MAPS system can measure different tool-centre points in the same working area. This allows getting the positional data of multiple handling systems in the same coordinate system, which can be aligned.

This paper describes occurring measurement errors and investigates the error sources. For this purpose, a simulation of the MAPS has been created. The advantage of this simulation is to explore the features of a maps image separately. Therefore, it is possible to find the error source by adding one feature after the other.

At the end of the proposed paper, the avoidance strategies for the described errors are discussed and presented to the reader.

References

[1] H. Schwenke, W. Knapp, H. Haitjema, A. Weckenmann, R. Schmitt, F. Delbressine, Geometric error measurement and compensation of machines—An update. *CIRP Ann.* **57**, 660–675 (2008).

[2] H. Kunzmann, T. Pfeifer, R. Schmitt, H. Schwenke, A. Weckenmann, Productive Metrology - Adding Value to Manufacture. *CIRP Ann.* **54**, 155–168 (2005).

[3] S. Sartori, G. X. Zhang, Geometric Error Measurement and Compensation of Machines. *CIRP Ann.* **44**, 599–609 (1995).

[4] S. Aguado, D. Samper, J. Santolaria, J. J. Aguilar, Identification strategy of error parameter in volumetric error compensation of machine tool based on laser tracker measurements. *Int. J. Mach. Tools Manuf.* **53**, 160–169 (2012).

[5] B. Ã. Shirinzadeh, P. L. Teoh, Y. Tian, M. M. Dalvand, Y. Zhong, H. C. Liaw, Robotics and Computer-Integrated Manufacturing Laser interferometry-based guidance methodology for high precision positioning of mechanisms and robots. *Robot. Comput. Integr. Manuf.* **26**, 74–82 (2010).

[6] K. Lau, R. J. Hocken, W. C. Haight, Automatic laser tracking interferometer system for robot metrology. *Precis. Eng.* (1986), doi:10.1016/0141-6359(86)90002-4.

[7] A. Nubiola, I. A. Bonev, Absolute calibration of an ABB IRB 1600 robot using a laser tracker. *Robot. Comput. Integr. Manuf.* **29**, 236–245 (2013).

[8] L. Pérez, Í. Rodríguez, N. Rodríguez, R. Usamentiaga, D. F. García, Robot guidance using machine vision techniques in industrial environments: A comparative review. *Sensors (Switzerland)*. **16** (2016), doi:10.3390/s16030335.

[9] S. Gharaaty, T. Shu, W. F. Xie, A. Joubair, I. A. Bonev, Accuracy enhancement of industrial robots by on-line pose correction. *2017 2nd Asia-Pacific Conf. Intell. Robot Syst. ACIRS 2017*, 214–220 (2017).

[10] S. Kyle, Alternatives in 6DOF probing - more flexibility , lower cost , universal? *Proc. 21st Annu. Coord. Metrol. Syst. Conf.* **m** (2005).

[11] D. Rieke-zapp, W. Tecklenburg, J. Peipe, H. Hastedt, C. Haig, Evaluation of the geometric stability and the accuracy potential of digital cameras — Comparing mechanical stabilisation versus parameterisation. *ISPRS J. Photogramm. Remote Sens.* **64**, 248–258 (2009).

[12] M. A. Amdal, Knut, Single camera system for close range industrial photogrammetry. *Int. Arch. Photogramm. Remote Sens.* **29**, 6–10 (1993).

[13] K. Lau, R. J. J. Hocken, A Survey of Current Robot Metrology Methods. *CIRP Ann.* **33**, 485–488 (1984).

[14] T. Luhmann, Close range photogrammetry for industrial applications. *ISPRS J. Photogramm. Remote Sens.* **65**, 558–569 (2010).

[15] T. Luhmann, Precision potential of photogrammetric 6DOF pose estimation with a single camera. *ISPRS J. Photogramm. Remote Sens.* **64**, 275–284 (2009).

[16] E. Hecht, *Eugene Hecht* (2002).

[17] M. Young, Pinhole Optics. *Appl. Opt.* **10**, 2763 (1971).